Top quark pair production cross-section in proton-proton collisions at √s = 7 TeV

Tsiakiris, M.

Publication date
2012

Chapter 3

Triggering on muons

"Physics is, hopefully, simple.
Physicists are not."

Edward Teller
1908 - 2003

The real-time selection of events is an essential step for the ATLAS experiment. As discussed in section 2.3, this task is assigned to the three-level trigger system with the main consideration of bringing the initial collision rate down to an acceptable write-out level, of typically 200 Hz, without throwing away interesting events. The T/DAQ system, ultimately, should ensure the stable and efficient selection of the interesting physics signatures and storing of the data for later (offline) analysis

In this chapter, we present the part of the trigger that is responsible for the identification of muons. In section 3.1 an overview of the reconstruction of muons at the trigger level is given. In section 3.2 we show the performance of the muon trigger system by analyzing the very first 7 TeV proton-proton collision data provided by the LHC. Lastly, we discuss in section 3.3 the possibility of measuring the trigger efficiency directly from data. We provide a feasibility study using the so-called *tag-and-probe* method, based on part of the collected data, and we show how the extracted result can be applied to the $t\bar{t}$ cross-section measurement.

3.1 Muon online reconstruction

Online reconstruction refers to the reconstruction and identification of objects that takes place within the TDAQ system. The main priority at this level is to be robust and efficient within tight time intervals and at the same time provide accurate measurements of the kinematics of the traversing objects. The three trigger layers (L1, L2 and EF) have different input rate tolerance and output rate requirements. So, different techniques are required at each level. Muon reconstruction at the trigger level depends mainly on information from the Muon Spectrometer and the Inner Detector, with the latter available only at the High Level Trigger (HLT).

3.1.1 The L1 Muon Trigger

At the L1 trigger [110] the muon selection depends solely on the information acquired by the RPCs and TGCs; a brief description of the technical details of the two technologies is already given in 2.2.5. As discussed in section 2.3.1, the small time window available for the L1 trigger

to make a decision does not allow a complete reconstruction of a muon track. Instead, it uses the hits seen by the chambers to translate them into trajectories based on their topology. We explain the method in detail in the following:

- Firstly, an infinite momentum trajectory is defined, i.e. a trajectory that starts from the nominal interaction point and traverses the Muon Spectrometer in a straight line by passing through a reference point. The reference point is determined based on the collected hits on one of the detector's layer, the *pivot*.
- Secondly, the deviations between all the observed hits and the straight line trajectory are measured.
- Lastly, the calculated deviations are compared with Look-Up Tables (LUT), obtained from Monte Carlo, which map the result to certain p_{T} intervals.

Eventually, all track candidates are collected and counted according to their assigned p_{T} intervals. This information is subsequently sent to the CTP where the L1 items are formed (see section 2.3.1).

RPC trigger

As discussed in section 2.2.5, the RPCs trigger on muons that traverse the barrel region of the Muon Spectrometer ($|\eta| \leq 1.05$). They are arranged in three layers and they are capable of measuring in both the η and the ϕ planes. An illustration of the RPC trigger can be seen in figure 3.1.

The low-p_{T} triggers begin with a hit at the middle RPC (pivot) which acts as the reference point for the infinite momentum trajectory. Further hits are then searched in the other RPC planes but within a specified region of certain width along each of the η and ϕ planes; this is called the *road*. The center of the road coincides with the infinite momentum trajectory while the size of the width depends on the evaluated p_{T} threshold; the higher the threshold, the smaller the width. For low-p_{T} triggers only the inner layer (RPC1) and the pivot is used and a coincidence of 3-out-of-4 hits per direction is required for the track to be considered. Depending on the size of the width that is used for including the track coincidence hits, the p_{T} is assigned. As mentioned earlier, the correlation between the road widths and different p_{T} thresholds is pre-computed from Monte Carlo and is placed in LUTs

The procedure for the high-p_{T} trigger is almost identical as for low-p_{T}, with the only exception that also hits in the outer plane (RPC3) are searched for. Furthermore, the coincidence of hits is 1-out-of-2 per direction for the outer layer, in addition to the requirement for the low-p_{T} trigger.

TGC trigger

The TGCs are responsible for triggering on muon candidates at the end-caps of the Muon Spectrometer. They are assembled in four layers and can measure both in the radial (R) and the azimuthal (ϕ) directions. Their acceptance limit, of $|\eta| \leq 2.4$, also defines the acceptance of the muon trigger for the ATLAS detector. A more detailed technical description of the layout is given in section 2.2.5. An illustration of the TGC trigger is shown in figure 3.2.

The triggering procedure on TGCs follows the same steps as in the RPC case. The pivot plane is now taken to be the outermost layer of TGCs (TGC3). Once a hit is found in the pivot plane, the algorithm searches for hits in the other TGC layers. For low-p_{T} thresholds only the two outermost layers (TGC2 and TGC3) are used and a coincidence of 3-out-of-4 is required in both directions, else the track is not considered. The p_{T} assigned to the track

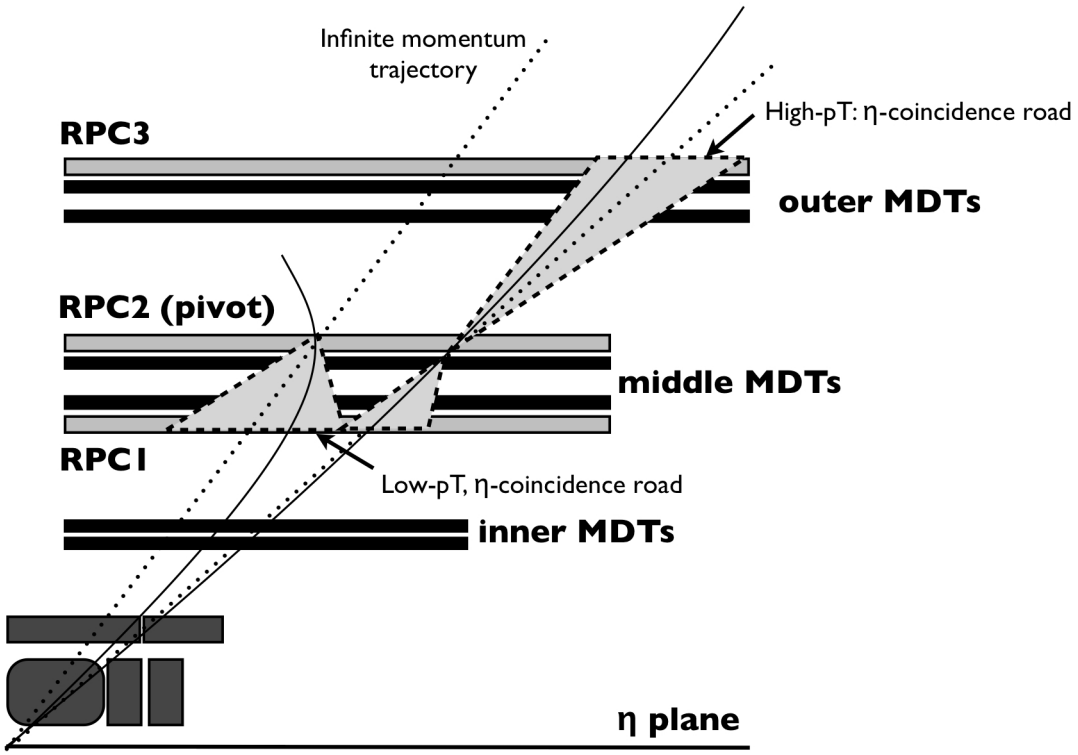

Figure 3.1: *Illustration of the RPC trigger at L1 identifying low-p_{T} and high-p_{T} tracks at the η (bending) plane.*

works in the same way as for the RPCs.

For the high-p_{T} thresholds, hits on the TGC layer right before the middle MDTs (TGC1) are also required. In this case a coincidence of hits of 2-out-of-3 in the radial plane and 1-out-of-2 in the azimuthal plane in TGC1 is required on top of the low-p_{T} coincidences. Note that the innermost TGC layer (inner TGC) has not been used throughout the 2010 data-taking period.

3.1.2 The L2 Muon Trigger

Starting from the L2, the Trigger is able to run software-based feature extraction algorithms (FEX) on the Regions-of-Interest (RoI), selected by the L1, and reconstruct the tracks of the traversing muons partially or completely. At this level, information from the Inner Detector becomes available allowing for a more accurate estimation of the p_{T} of the muons and an increased rejection rate of fakes. Also, information from the MDTs precision chambers become available at this level. The main FEX algorithms are: `muFast` [111, 112] and `muComb` [113]. These will be discussed below.

Additional algorithms are also implemented, oriented to more specific event signatures, usually employed in parallel to the main algorithms. Such examples are the `muIso` [113, 114], which can determine the isolation around a muon track by accessing calorimetry information, or the `muTile` [113, 115], which utilizes hadronic calorimeter information to determine the presence of low-energy muons, typically interesting for B-physics searches. These algorithms are not discussed further on.

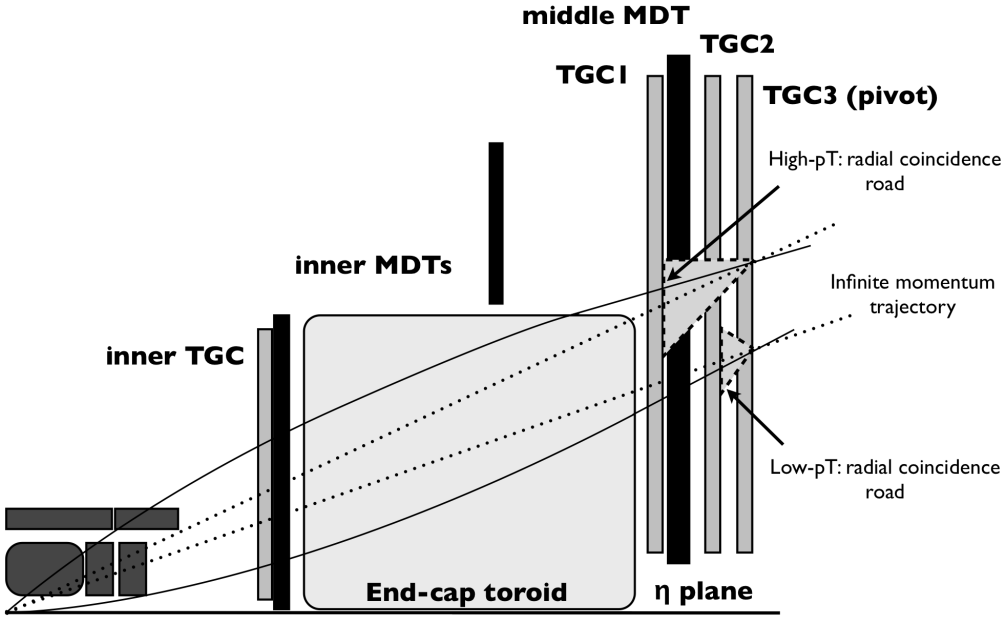

Figure 3.2: *Illustration of the TGC trigger at L1 identifying low-p_{T} and high-p_{T} tracks at the radial (bending) plane.*

The standalone track algorithm - `muFast`

Among the various algorithms at L2, `muFast` [111, 112] is the first algorithm that is invoke and only uses hit information obtained from the Muon Spectrometer, specifically from the RPCs, TGCs and the MDTs. For the barrel region the reconstruction steps are the following:

- **Pattern recognition:** Based on the Region-of-Interest found by the L1 trigger, a pattern recognition algorithm is ran. At first the pattern recognition is applied on RPC hits and determines a road around the candidate muon trajectory. This result serves as input to the MDT pattern recognition where hits not associated with the muon trajectory are rejected (background hits).
- **Straight line fit:** At each MDT station, a straight-line track fit is performed based on the tubes that were selected by the pattern recognition. The drift-time measurements are exploited and the independent fits provide up to three precision points, one at each MDT layer, taken from the middle of the straight-line tracks. The curvature of the track and its sagitta (s) is estimated based on these precision points.
- p_{T} **assignment:** Following the sagitta measurement, the p_{T} of the track is found with pre-computed LUTs, hence avoiding time-consuming fit methods. The LUTs are basically an $\eta - \phi$ map which, assuming that tracks originate from the nominal interaction point, follows the relation:

$$\frac{1}{s} = A_0 \cdot p_{\mathrm{T}} + A_1 \ , \tag{3.1.1}$$

  where A_0 depends on the Muon Spectrometer alignment and the magnetic field of the toroid, and A_1 corrects for the energy loss in the calorimeters. Both parameters are estimated from Monte Carlo and can, naturally, vary for different $\eta - \phi$regions.

A modified approach is followed for the end-cap regions with the main difference being in the computation of the track's p_{T}. Equation 3.1.1 is only valid in case of a homogeneous field

where the trajectory in the plane perpendicular to the field can be considered circular. This is not the case for magnetic field in the end-caps, i.e. the trajectory is not a helix. Two angles are defined for estimating the p_{T}. The angle α for low-p_{T} tracks, which is defined as the angle between the direction of the muon track (slope) in the middle layer MDTs and the direction of an infinite momentum track. The angle β for high-p_{T} tracks, which is defined as the angle formed by the inner MDT track and the middle MDT track. In each case, the p_{T} is obtained from LUTs which are based on the following linear relation:

$$\frac{1}{p_{\mathrm{T}}} = A_x \cdot x + B_x, \ , \tag{3.1.2}$$

where x is either α or β. The parameters A_x and B_x depend on the position of the track and are extracted from Monte Carlo. Finally, the output of `muFast` is a list of features including the track's coordinates and its transverse momentum. These are then used by hypothesis algorithms which form a decision (accept or reject) for the event (see section 2.3.6).

The combined track algorithm **-** `muComb`

The `muComb` algorithm combines the tracks found in the Muon Spectrometer with the ones found by the Inner Detector. This gives good rejection power on muons that originate from decaying-in-flight particles (e.g. $\pi^+ \to \mu\nu$ or $K^+ \to \mu\nu$) and reduces the amount of fakes that originate from cavern background.

The reconstruction procedure of `muComb` requires that both a Muon Spectrometer and an Inner Detector track exist. For the former, the track is already calculated by the `muFast` algorithm that precedes, while for the latter the result is obtained from the `IDSCAN` algorithm [113]. The `IDSCAN` algorithm receives the three-dimensional space points from the Pixel and the SCT detectors as input and performs the following tasks:

- **z-finder:** Initially, the algorithm estimates the z-position of the primary vertex. This is done in three steps. Firstly, the observed hits are divided in ϕ-windows and hit pairs are made for each window. Secondly, the hit pairs are extrapolated to the beam line and their z-position is put in a histogram. Finally, the z value is extracted from the histogram by integrating the region with the most entries over all the ϕ windows.
- **Hit Filter:** The algorithm identifies clusters of hits (groups) in an $\eta - \phi$ grid by considering all those that are related with tracks originating from the estimated z-position. During this process, hits that may originate from pile-up or noise are effectively filtered out. For a group to be considered, hits must be found in multiple layers of the SCT and Pixel detectors.
- **Group Cleaner:** At this stage the groups are cleaned from duplicated hits and possible noise. Subsequently, track candidates are formed. Each triplet of hits is considered as a candidate and an initial estimate of its p_{T}, ϕ_0 and d_0 is made. After applying certain quality cuts groups of candidates are made.
- **Track Fitter:** The last step is to run the fitting algorithm on the track candidates. The fit is performed by the Kalman-filter fitter [116, 117, 118] and returns the space points of the track, the relevant track parameters and the error matrix.

The `muComb` algorithm combines the information obtained from the Muon Spectrometer and the Inner Detector. It first extrapolates tracks, from each of the two sub-detectors, to a common virtual surface: a cylinder around the beam-line at the entrance of the Muon Spectrometer. Initially, a pre-selection is performed on the Inner Detector tracks based on spatial matching with the `muFast` tracks. The matching windows are optimized with the help

of Monte Carlo simulated samples. Subsequently, each pre-selected track is combined with the standalone track and a p_{T} estimate is made. The p_{T} is in fact a resolution-weighted average. For each combination a χ^2 of the fit is obtained and the one with the minimum value is considered to be the best candidate.

3.1.3 The EF Muon Trigger

At the EF level the trigger is able to run a complete track reconstruction within the time window available for a decision. As a result, the algorithms are in fact wrappers of the actual offline reconstruction software, modified to be able to run on the Trigger system. Two main algorithms exist: the `TrigMuonEF` and the `TrigMuGirl` [113, 119].

The outside-in algorithm - `TrigMuonEF`

The `TrigMuonEF` algorithm provides complete track reconstruction by running four sequential steps: the `SegmentFinder`, the `TrackBuilder`, the `Extrapolator` and the `Combiner`. At each step, the corresponding offline reconstruction algorithm runs based on either the `MOORE` [120] or the `MuID` [121] reconstruction software.

`MOORE` is responsible for reconstructing the tracks in the Muon Spectrometer. It identifies regions with hit activity in both MDTs and trigger chambers and applies a pattern recognition algorithm. Subsequently a track fitting procedure is performed on the selected hits. In addition, it takes energy losses from traversing the calorimeter, as well as Coulomb scattering effects into account. The final reconstructed track is expressed with respect to its entry point in the Muon Spectrometer. Within the `TrigMuonEF` implementation the above tasks are performed by the `SegmentFinder` and the `TrackBuilder`.

On the other hand, `MuID` is responsible for associating tracks found by `MOORE` with tracks found in the Inner Detector. Calorimeter information is used as well. At first, the algorithm refits the Muon Spectrometer track such that it is expressed with respect to the production vertex. These tracks are then matched with Inner Detector tracks and a combined fit is performed to all successful matches. The `TrigMuonEF` implementation wraps the above functionality in the `Extrapolator` and the `Combiner` steps.

An important advantage of the `TrigMuonEF` is its ability to run in both "full scan" and "seeded" mode. The first is practically the same as the offline reconstruction where the complete detector information is available. In the second mode, the EF algorithms are only ran on identified RoIs that seed the EF. The seeding typically comes from the L2 trigger, however for debugging purposes it may also be provided by the L1 trigger. Due to the step-wise procedure that begins at the Muon Spectrometer and extrapolates to the Inner Detector, the `TrigMuonEF` can be seen as an "outside-in" reconstruction strategy.

The inside-out algorithm - `TrigMuGirl`

Similar to the `TrigMuonEF`, the `TrigMuGirl` algorithm is also based on the offline reconstruction software of `MuGirl`. The algorithm begins with track candidates found in the Inner Detector. Those tracks are then extrapolated to the Muon Spectrometer and the algorithm searches for hits in the vicinity of the estimated trajectory. Segments are constructed from the found hits and are then used to improve the extrapolated track. The final muon track is estimated by a global fit on the initial Inner Detector track and the respective Muon Spectrometer hits. The `TrigMuGirl` algorithm is seeded by Inner Detector tracks and as a result it must be based on the result of the L2 combined algorithm. This implementation of the Event Filter, although initially considered for first analyses, is not used in this thesis and thus not

discussed further on.

3.2 Performance of the muon trigger with the first data

The first proton-proton collisions at a 7 TeV center-of-mass energy were delivered by the LHC to the ATLAS detector in early 2010. Up until the end of July 2010, the luminosity of the beams was low enough, reaching a peak of just $3 \cdot 10^{30} cm^{-2} s^{-1}$, to allow the trigger system to apply only a minimal rejection of events. This had the advantage of establishing an inclusive muon sample with minimum kinematic biases, which is well suited for testing the performance of the trigger.

3.2.1 Data sample and selection of muons

In order to accommodate the changes that may take place during the data-taking, each run in ATLAS belongs to a period (A through I, for 2010) and a sub-period (numerically defined within a period). Each period corresponds to a number of data-taking runs in which the accelerator, the trigger of the detector and the detector as a whole were left in the same configuration. The data used in this section of the thesis are obtained from period B up to period D1. The selected events are required to be recorded with all the Muon Spectrometer and Inner Detector components in operation and in addition with the magnetic fields of both the solenoid and the toroid magnets at their nominal values. The total integrated luminosity under these conditions is estimated at about 50 nb^{-1}, as shown in table 3.1.

Period	$\int \mathcal{L} dt$ (nb^{-1})	**Date (in 2010)**
B (1-2)	9.2	23^{rd} April - 17^{th} May
C (1-2)	9.6	17^{th} May - 5^{th} June
D1	30.9	27^{th} June - 1^{st} July
All Periods	49.70	

Table 3.1: *Total integrated luminosity registered by ATLAS for the data periods of interest.*

Event selection

The performance of the trigger is tested on a muon enriched sample that is collected with minimal kinematic biases introduced. At the trigger level, events are selected based on a muon "full-scan" trigger that follows the chain:

$$\texttt{L1\_MBTS\_2} \rightarrow \texttt{EF\_mu4\_MSonly\_MB2\_noL2\_EFFS}\ .$$

The `L1_MBTS_2` item is a Minimum Bias trigger based on sets of scintillators that are placed next to the cryostats of the Liquid Argon calorimeter end-caps, covering the region of $2.0 \leq |\eta| \leq 3.8$. The only requirement for acceptance is to have at least two independent signals in each end-cap scintillator set. Effectively, this trigger fires when collision events take place at the time of an expected bunch-crossing, thus it reduces the rate of non-collision background events. After the acceptance of the L1 item, the event is evaluated by the Event Filter, entirely bypassing L2 processing. At the EF level, the `TrigMuonEF` algorithm is applied to find candidate muon tracks within the full coverage of the Muon Spectrometer. Thus, it is not seeded by an RoI and it doesn't try to combine tracks with the Inner Detector. Kinematically, the EF algorithm introduces as little bias as possible with no directional cuts applied and with

the p_{T} thresholds adjusted at the lowest expected transverse momenta for muons originating from the interaction point[1]; the actual η dependent thresholds are shown in table 3.2.

$\lvert\eta\rvert$ **bin**	p_{T} **threshold (GeV)**
$[0.00, 1.05]$	3.0
$(1.05, 2.50]$	2.5

Table 3.2: *Event Filter p_{T} thresholds for the trigger used in the selection of the muon-rich sample. Numbers taken from [122].*

In order to reject possible cosmic contamination, further refinement is done by requesting the reconstruction of a primary vertex. In addition, this vertex must have its z-position within 150 mm from the nominal interaction point ($z_{PV} < 150mm$) and at least three tracks must be associated with it ($N_{tracks} \geq 3$).

Muon selection

Offline reconstructed muons which are considered for the final event sample must be successfully combined from a Muon Spectrometer and an Inner Detector track, i.e. those muons defined as "combined" by the `MuID` reconstruction software are used. In addition, for a combined muon to be included it must satisfy all the following requirements:

- $p > 4$ GeV and $p_{\mathrm{T}} > 2.5$ GeV, which is the minimum requirement for a muon that has successfully traversed the calorimeters and has reached the Muon Spectrometer. This way possible contamination with fakes, originating by combining an Inner Detector track with a fake Muon Spectrometer track, is reduced.
- Number of hits in the SCT and Pixel layers: $N_{SCT} > 5$ and $N_{Pixel} > 0$, respectively. With these requirements we establish that the track is built from information from all the silicon detectors, assuring a good Inner Detector track quality.
- The matching between the Muon Spectrometer track and the Inner Detector track gives $\chi^2 < 50$, minimizing the ambiguity on the compatibility of the Inner Detector and Muon Spectrometer track components. The large threshold is justified by the fact that this is the beginning of the data-taking period and therefore large deviations may occur due to uncalibrated algorithms.

3.2.2 Performance measurements

The performance of both the L1 trigger and the HLT is examined primarily on their selection efficiency. For the purpose of this analysis the efficiency is defined as the ratio of muons accepted by the trigger (n_{trig}) over the total number of muons (n_{tot}). The n_{tot} is taken as all the muons passing the selection explained in the previous section and n_{trig} is taken as those that have are matched to a trigger object satisfying the respective trigger requirements; the n_{trig} is a subset of n_{tot}. Hence the following holds:

$$\epsilon = \frac{n_{trig}}{n_{tot}} \ . \tag{3.2.1}$$

[1] Muons produced at the interaction point, able to traverse the calorimeters and reach the Muon Spectrometer must have $p \geq 3$ GeV at $\eta \approx 0$ [93].

The efficiency depends on the selection requirements applied at the trigger level. The usual implementation is to simply accept or reject events based on their transverse momentum compared to a given threshold. The distribution of the efficiency with respect to the transverse momentum is usually referred to as the *turn-on curve* of a trigger. The transverse momentum used, is typically taken from the offline reconstruction as this is considered to be closer to the "true" value.

For a hypothetical trigger that fires above a certain p_{T} threshold (p_{T}^{thres}), the efficiency described in relation 3.2.1, in an ideal case, will follow a step-function, namely it will return an efficiency of 1 for $p_{\mathrm{T}} \geq p_{\mathrm{T}}^{thres}$ and 0 for $p_{\mathrm{T}} < p_{\mathrm{T}}^{thres}$. However, due to resolution effects the measured p_{T} at the trigger level may be smeared with respect to the offline reconstructed p_{T}, therefore altering the turn-on curve. Assuming that the resolution effects induce a gaussian behavior, the expected distribution would be of the following form:

$$f(x) = 0.5\alpha \left(1 + Erf\left(\frac{x-\beta}{\sqrt{2}\gamma}\right)\right) \ , \tag{3.2.2}$$

where x is the selection parameter (p_{T}) and $Erf(y)$ is a gaussian error function:

$$Erf(y) = \frac{2}{\sqrt{\pi}} \int_0^y e^{-t^2} dt \ . \tag{3.2.3}$$

The constant parameters are: α, which provides a measure of the plateau of the efficiency, namely the efficiency at value of the p_{T} well above the trigger threshold; β, the actual threshold of the trigger; γ, the slope in the turn-on region which is gives a measure of the smearing as it is equivalent to the gaussian σ. Naturally, additional effects that are not simply described by a gaussian resolution may still be present and often they may not be described simply by the above equation. In the following, we focus mainly on the result of the plateau measurement to illustrate the performance of trigger.

Level-1 efficiency

The efficiency of the L1 trigger is evaluated, with the muon sample selected as described in section 3.2.1, for the following trigger items: the `L1_MU0` which is configured with a low-p_{T} logic but with an 'open' road, the latter does not specify a road width in which coincidences are counted but it takes into account all the hits that fall within the same trigger tower ($\eta \times \phi \approx 0.1 \times 0.1$) thus maximizing acceptance and minimizing the p_{T} bias; the `L1_MU6` configured with a low-p_{T} logic accepting muons with p_{T} of at least 6 GeV; the `L1_MU10` configured also with a low-p_{T} logic and accepting muons with p_{T} of at least 10 GeV.

For establishing the connection between an offline reconstructed object and the trigger decision, the former is required to be matched to a corresponding trigger-level object. Only if such a match is successful and the trigger-level object has satisfied the trigger threshold requirements, the offline muon is considered a triggered muon. The matching itself is based on a $\Delta R = \sqrt{\Delta\eta^2 + \Delta\phi^2}$ metric with a cut threshold of $\Delta R \leq 0.3$. At L1, the decision is based only on Muon Spectrometer information, thus the kinematic variables of the offline reconstructed muon are taken from the Muon Spectrometer track. The turn-on curves for L1 are also created with respect to the p_{T} as measured by the Muon Spectrometer. In figure 3.3 we plot the results for the three trigger items separated in the barrel (RPC) and the end-cap (TGC) regions. Minimum Bias Monte Carlo events and single-muon Monte Carlo[2] events are also overlaid with the data, with the single-muon sample being generated with muons of

[2]The single-muon Monte Carlo events are simply muons that are generated from the nominal interaction point, distributed uniformly in $\eta - \phi$ and at different p_{T} intervals.

Trigger Item	Data (%)		MC (%)	
	RPC	TGC	RPC	TGC
L1_MU0	75.3 ± 0.2	94.2 ± 0.2	79.2 ± 0.8	96.4 ± 0.3
L1_MU6	75.8 ± 0.3	73.2 ± 0.4	78.7 ± 1.1	91.8 ± 1.1
L1_MU10	74.2 ± 0.5	75.4 ± 0.9	74.7 ± 1.9	93.5 ± 1.7

Table 3.3: *Plateau efficiencies for L1 trigger items as estimated by fitting the function 3.2.2 on the turn-on distributions. All uncertainties are statistical only and are obtained from the fit.*

$p_{\mathrm{T}} > 6$ GeV. With the function described in equation 3.2.2, each of the curves provides an estimate of the efficiency plateau at each trigger item; the results are shown in table 3.3.

A number of observations can be made. First of all, the generally lower efficiency observed in the RPCs, compared to ones in the TGCs, is because of the reduced geometrical acceptance of the former. In the barrel region, primarily due to the cabling hole at approximately $\eta \approx 0$, the acceptance is estimated to be about 80%, while in the end-cap regions it is 95%. The reason why the offline reconstruction still finds these muons is because of optimized reconstruction which includes extensive information, by taking into account the Inner Detector or even in certain cases the Calorimeters, and can successfully reconstruct their tracks. Secondly, all the RPC triggers and the TGC open-road trigger show to be very close to the expected plateau limits with only a maximum of 4% difference which is accounted as detector inefficiencies. However, for the TGCs, when a road width is applied (triggers `L1_MU6` and `L1_MU10`), a large deviation from the expected acceptance is observed, an effect that is only present in the data sample. The reason for this was found to be the TGC chamber cross-talk at the direction of the strips, namely hits that could also be found in strips neighboring the actual muon track. If such a hit is found, its position may be used instead of the real track hit for defining the coincidence window in ϕ and naturally the result after counting the coincidences may differ significantly. As this effect worsens the ϕ resolution, it also has an effect in the counting of n_{sel} which depend on the matching between trigger and offline. In the end, the solution, which was also incorporated for subsequent data-taking periods, is to increase the road width in the ϕ direction, thus increasing the acceptance of the trigger. The reason that this effect does not appear in the Monte Carlo events is because the simulation is modeled with a lower cross-talk probability A detailed description of the effect along with the proposed solution and the results after the optimization of the road is presented in [123].

HLT efficiency - Standalone triggers

The performance of the HLT is first tested at the Muon Spectrometer only, i.e. the standalone triggers. We examine the efficiency of the L2 Muon Spectrometer algorithm with respect to the seeding L1 trigger item and subsequently the equivalent Event Filter algorithm with respect to the L2 selection. The L2 algorithms under consideration are: the `L2_mu4_MSonly` which is seeded by `L1_MU0`, the `L2_mu6_MSonly` seeded by `L1_MU6` and the `L2_mu10_MSonly` seeded by `L1_MU10`. Respectively for the Event Filter the `EF_mu4_MSonly`, `EF_mu6_MSonly` and `EF_mu10_MSonly` are examined. The applied thresholds for the above triggers are shown in table 3.4. Similar to what happens with the L1, the offline muons are matched with the L2 `muFast` or EF `TrigMuonEF` objects that satisfy the hypothesis criteria of the trigger algorithms and the sample of trigger-selected muons is obtained. As these algorithms are based on Muon Spectrometer information their efficiency is given with respect to the track p_{T} estimated by this sub-detector. In figure 3.4 we plot the L2 result separated in the RPC and TGC regions,

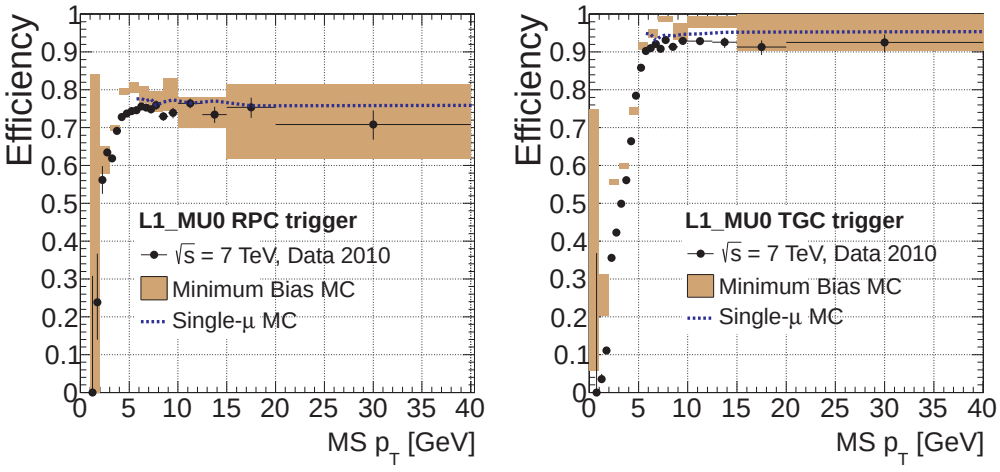

(a) *The `L1_MU0` trigger configured with a low-p_{T} logic and an 'open' road.*

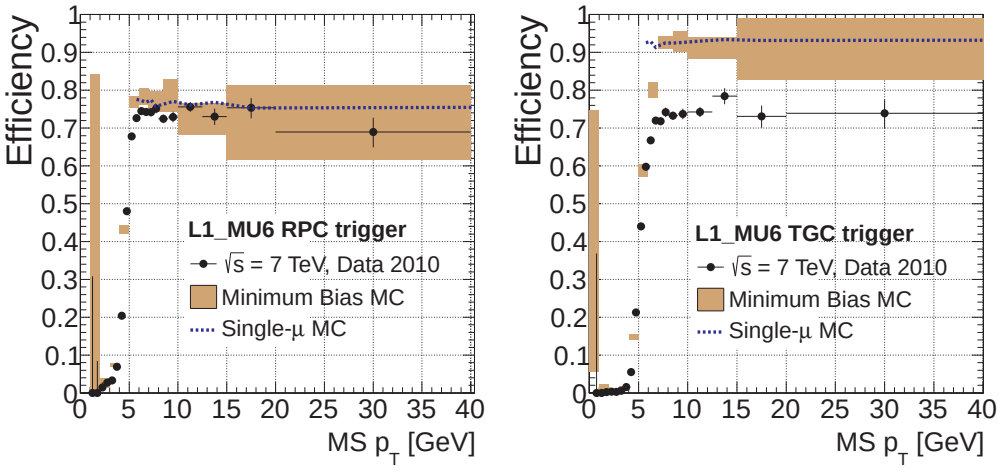

(b) *The `L1_MU6` trigger with a low-p_{T} logic applied.*

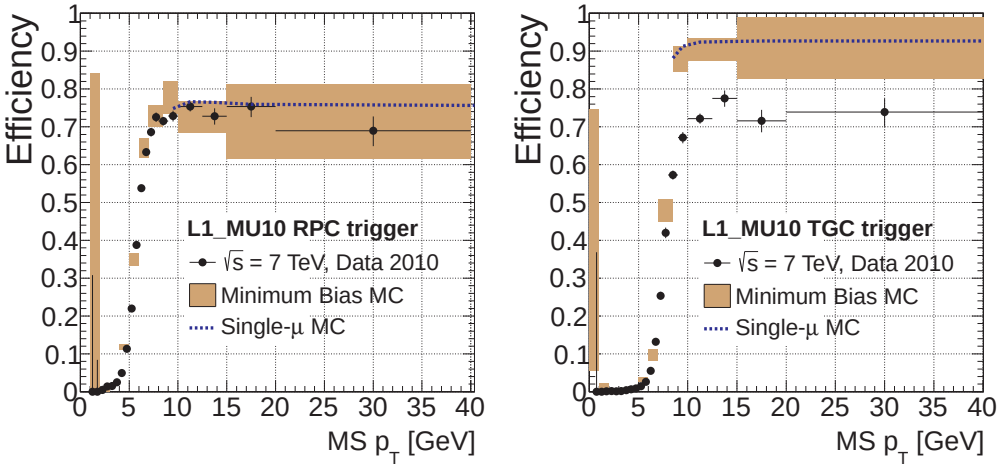

(c) *The `L1_MU10` trigger with a low-p_{T} logic applied.*

Figure 3.3: *The L1 turn-on curves for three different trigger items with a low-p_{T} configuration. The efficiency is shown with respect to the p_{T} of the offline reconstructed Muon Spectrometer track and is separated in the RPC, $|\eta| < 1.05$ region (left), and the TGC, $|\eta| > 1.05$ region (right).*

$\|\eta\|$ bin	p_{T} thresholds for L2 and EF (GeV)		
	mu4_MSonly	mu6_MSonly	mu10_MSonly
[0.00, 1.05]	3.0	5.4	8.9
(1.05, 1.50]	2.5	4.5	9.0
(1.50, 2.00]	2.5	4.9	8.4
(2.00, 2.50]	2.5	5.3	9.2

Table 3.4: *The L2 and Event Filter p_{T} thresholds applied for the three Muon Spectrometer-only triggers that are tested. Numbers taken from [122].*

since small differences between them exist especially in the estimated track p_{T}. In figure 3.5 we plot the EF results for the full detector coverage. The reason for not separating in RPC and TGC in this case is because the same algorithm is applied throughout, irrespectively of the muon's η coordinate, while in the case of the L2, differences exist in the determination of the p_{T}.

As the L2 efficiency is estimated based on the L1 selected sample, the geometrical effects are absent and the expected efficiency is closer to 100%. The same applies for the Event Filter when examined with respect to the L2. For the L2, the plateau efficiency of the turn-on curves is between 90% and 100%. The agreement between data and Monte Carlo is in general good although the data exhibit a slightly lower plateau efficiency than what the Monte Carlo anticipate. This difference is attributed to the non-optimized LUTs that were used in the early data due to the lack of knowledge with respect to the alignment of the Muon Spectrometer [124]. Another effect that is observed is that a fraction of muons below the threshold are successfully passing the `L2_mu6_MSonly` and `L2_mu10_MSonly` trigger requirements. For the TGCs, where the effect is more pronounced, it is attributed to the complex and inhomogeneous magnetic field in the end-caps, especially in the transition regions which worsens the p_{T} resolution [124]. Additionally, and what is mainly the case for the RPCs, mis-matching of muons may lead to such effects.

For the Event Filter, the first important observation is that the turn-on builds faster that in the case of the L2 as a result of the better resolution that can be achieved. Additionally, the plateau efficiency is reaching the expected 100% and is well in agreement with the Monte Carlo. Lastly, the effect with the lower-than-threshold muons is again observed although less severe in terms of efficiency and with lower statistics, practically indicating the better rejection power at the Event Filter.

HLT efficiency - Combined triggers

At the next step, we test the performance of the algorithms that are based on combination of the Inner Detector and Muon Spectrometer track. Namely, the `L2_mu4`, `L2_mu6` and `L2_mu10` at the L2, and the `EF_mu4`, `EF_mu6` and `EF_mu10` at the Event Filter. In each case, the relevant L2 algorithm (`muComb`) is tested with respect to its seed, the L2 Muon Spectrometer algorithm (`muFast`) and then the Event Filter combined algorithm is tested with respect to the L2 combined algorithm. As these algorithms are based on the combined track the turn-on curves are estimated with respect to the offline reconstructed combined track. The thresholds applied in each case by the hypothesis algorithms are shown in table 3.5.

Figure 3.6 shows the resulting efficiency plots for the L2 and the Event Filter. Given that the reconstruction procedure is equivalent for both RPC and TGC regions no distinction is made. It is evident from the plots that the L2 achieves the expected plateau very close to

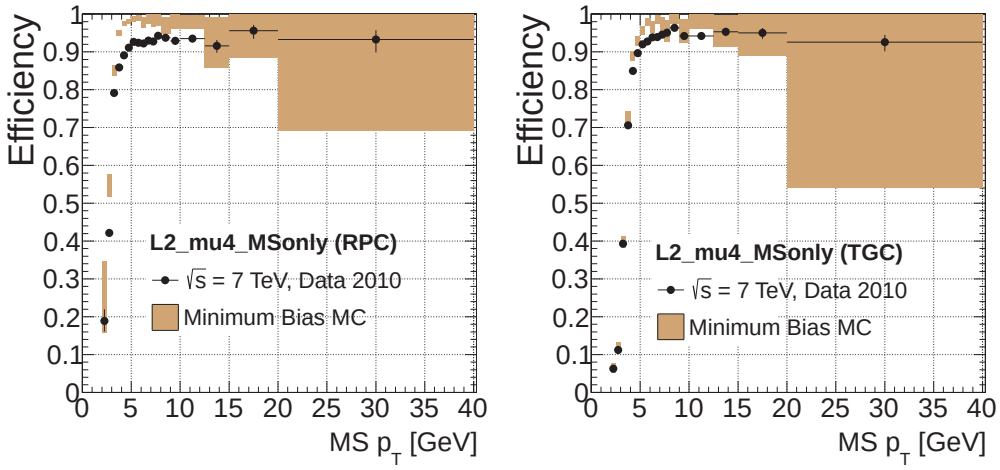

(a) *The* `L2_mu4_MSonly` *trigger seeded by* `L1_MU0`*.*

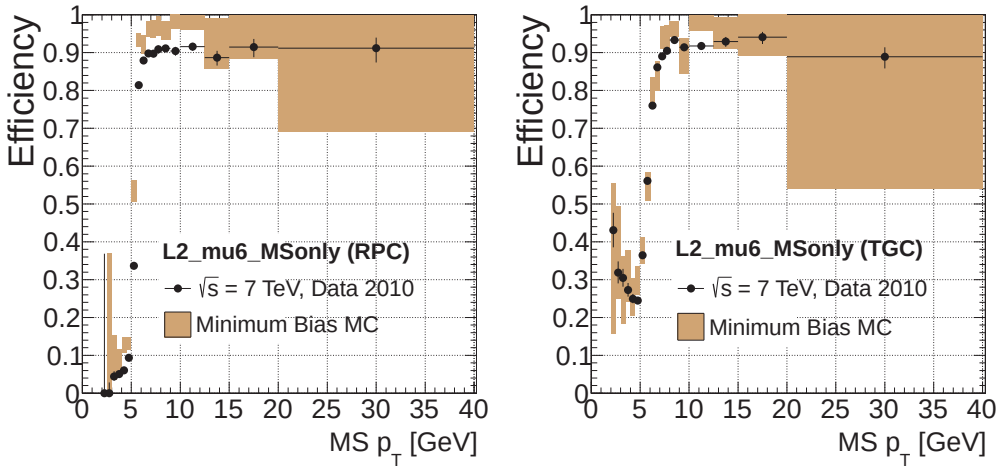

(b) *The* `L2_mu6_MSonly` *trigger seeded by* `L1_MU6`*.*

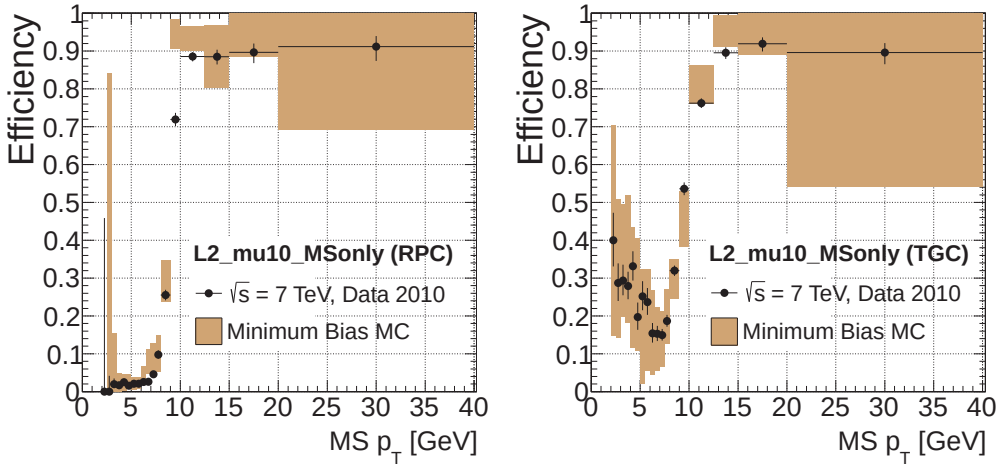

(c) *The* `L2_mu10_MSonly` *trigger seeded by* `L1_MU10`*.*

Figure 3.4: *The L2 RPC (left) and TGC (right) turn-on curves for* `L2_mu4_MSonly`*,* `L2_mu6_MSonly` *and* `L2_mu10_MSonly`*. The efficiency is estimated relative to the L1 trigger items and with respect to the offline Muon Spectrometer track* p_{T}*.*

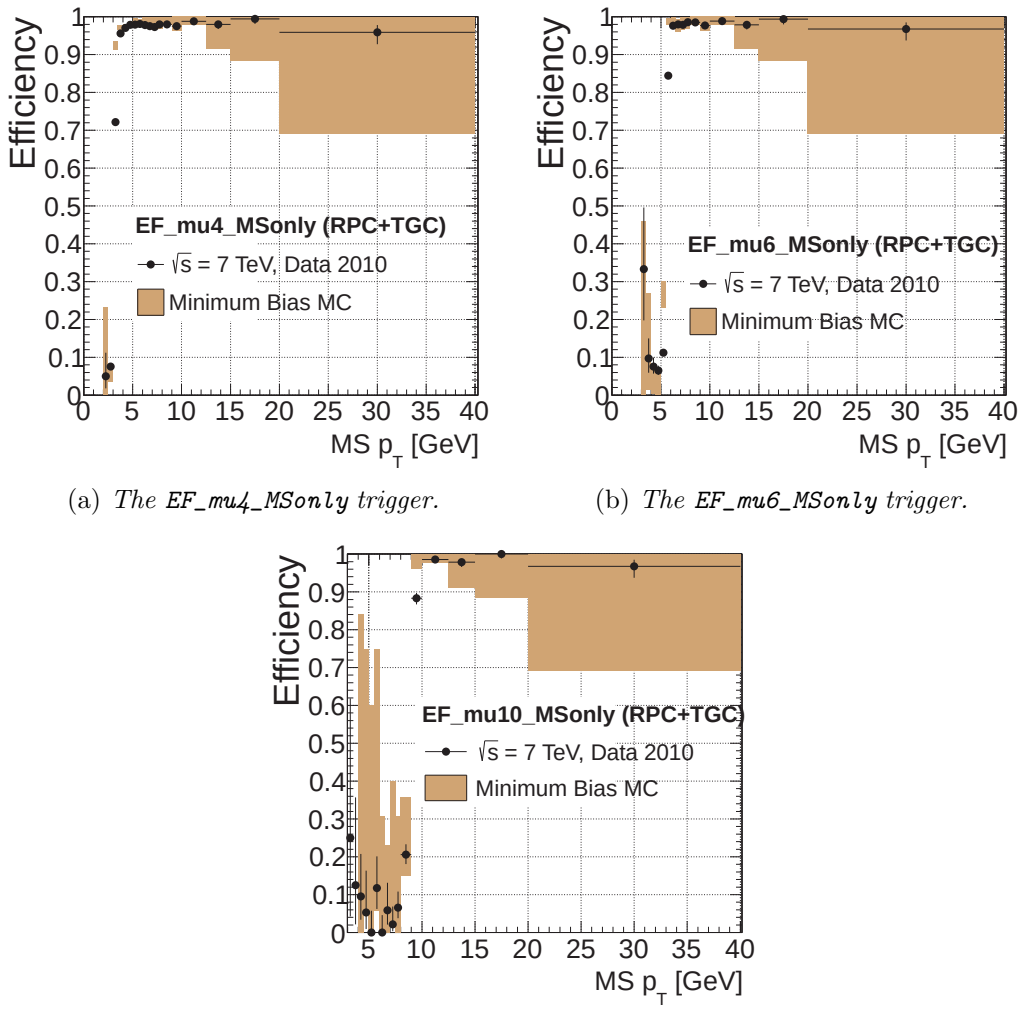

(a) *The* `EF_mu4_MSonly` *trigger.*

(b) *The* `EF_mu6_MSonly` *trigger.*

(c) *The* `EF_mu10_MSonly` *trigger.*

Figure 3.5: *The EF turn-on curves for* `EF_mu4_MSonly`*,* `EF_mu6_MSonly` *and* `EF_mu10_MSonly` *trigger . The efficiency is estimated relative to the L2 trigger and with respect to the offline Muon Spectrometer track* p_{T}*.*

$\lvert\eta\rvert$ **bin**	p_{T} **thresholds (GeV)**					
	`mu4_MSonly`		`mu6_MSonly`		`mu10_MSonly`	
	L2	**EF**	**L2**	**EF**	**L2**	**EF**
$[0.00, 1.05]$	3.0	3.93	5.8	5.88	9.8	9.77
$(1.05, 1.50]$	2.5	3.91	5.8	5.81	9.5	9.67
$(1.50, 2.00]$	2.5	3.88	5.8	5.78	9.6	9.62
$(2.00, 2.50]$	2.5	3.88	5.6	5.76	9.7	9.57

Table 3.5: *The L2 and Event Filter* p_{T} *thresholds applied for each of the combined triggers that are tested. Numbers taken from [122].*

100% efficiency, well in accordance with the Monte Carlo expectation. However, for the Event Filter it is observed that the plateau does not reach this value. In fact, the turn-on curve reaches a peak at the top of the slope, but a trend, in which for higher-p_{T} values the efficiency consistently drops, is observed. This is not the same effect as the statistical fluctuations observed in figures 3.4 and 3.5. This has been attributed to the absence of the alignment constants at this level of the trigger reconstruction which leads to an erroneous measurement of the p_{T} [125].

Residual distribution and algorithm resolution

The performance of an individual algorithm can be assessed by comparing the value of the transverse momentum at the trigger level with the one measured from the offline reconstruction. We use the following residual relation:

$$r = \frac{1/p_{\mathrm{T}}^{offline} - 1/p_{\mathrm{T}}^{trigger}}{1/p_{\mathrm{T}}^{trigger}}, \tag{3.2.4}$$

where the $p_{\mathrm{T}}^{offline}$ is the offline reconstructed transverse momentum and $p_{\mathrm{T}}^{trigger}$ is the transverse momentum as measured by the respective trigger algorithm. The residual distribution typically has a gaussian shape, as for example in figure 3.7 where the L2 `muComb` p_{T} residual is shown for the range of 6-8 GeV. Fitting a gaussian function on the resulting plots determines the mean of the residual distribution while the sigma provides the achieved resolution of the respective trigger algorithm with respect to the offline. In figure 3.8 the resulting residual mean and resolution is shown for each of the `muFast`, `muComb` and `TrigMuonEF` algorithms. For the latter, the combined measurement is used.

The result on the residuals of the `muFast` algorithm (figure 3.8(a)) shows a significant offset of the mean of the residual for the end-cap regions, consistent in both data and Monte Carlo. This is because the measurement exhibits large tails towards negative values. These are the result of the complex and inhomogeneous magnetic field regions of the end-caps which is only approximated for the determination of a track's p_{T}. Naturally, the resolution is also affected resulting in much higher values than in the RPC. Generally, the agreement between Monte Carlo and data is observed to be good indicating that the simulation describes these effects sufficiently well. The inclusion of the combined track is expected to provide a measurement at the trigger level which is closer to the expected offline reconstructed result. The result on the `muComb` algorithm (figure 3.8(b)) shows indeed values close to zero but with large deviation at low energy muons. Nevertheless, it is evident that the achieved resolution is considerably improved The differences that are shown to exist between Monte Carlo and data, indicate the need for a better understanding of the momentum scale of the algorithms. Finally, the `TrigMuonEF` result (figure 3.8(c)) shows an even better reconstruction performance by the Event Filter which is expected as the offline and the Event Filter reconstruction share the same algorithms. It should be noted that at the EF a larger difference in the resolution is observed between Monte Carlo and data. This, as has been said, is attributed to the absence of proper calibration constants at the EF combined triggers.

3.3 Data-driven trigger efficiency measurement

Estimating the efficiency with which a trigger is selecting events, is an important step in every analysis that requires knowledge on the exact amount of collected data. In the previous section the efficiency measurements presented were estimated by counting the number of muons that were passing a given trigger threshold and comparing it with the total number of candidates.

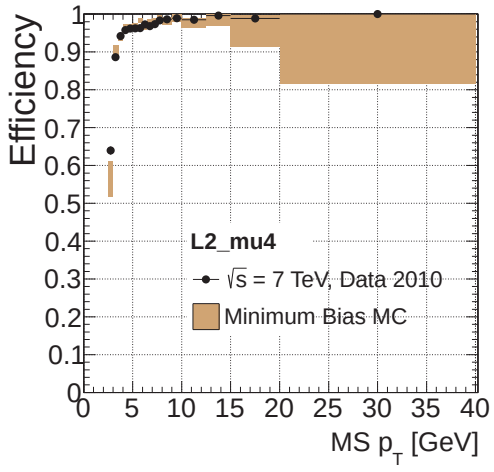

(a) *The* `L2_mu4` *trigger.*

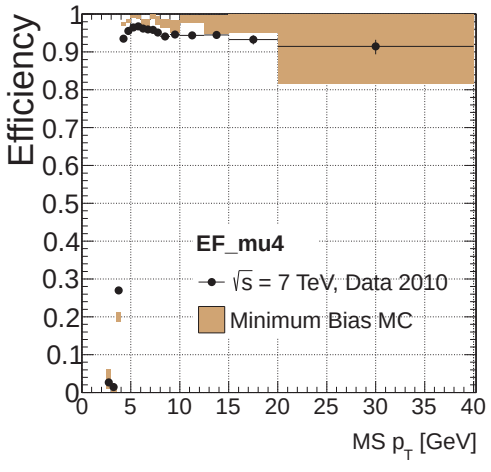

(b) *The* `EF_mu4` *trigger.*

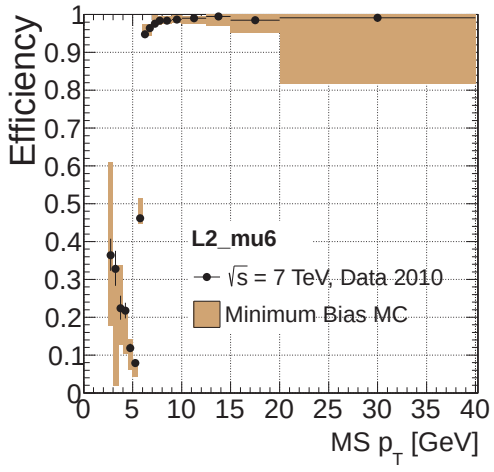

(c) *The* `L2_mu6` *trigger.*

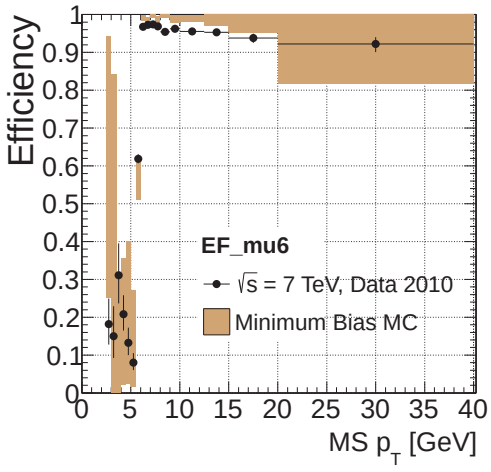

(d) *The* `EF_mu6` *trigger.*

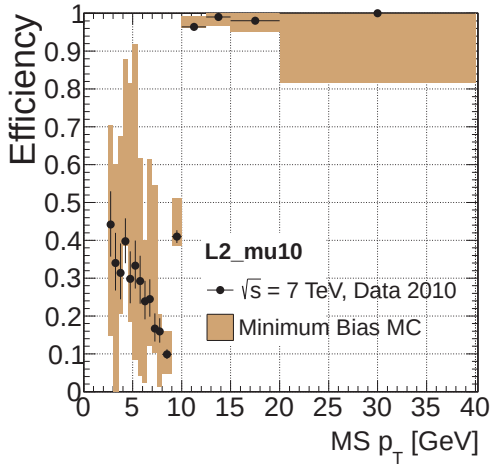

(e) *The* `L2_mu10` *trigger.*

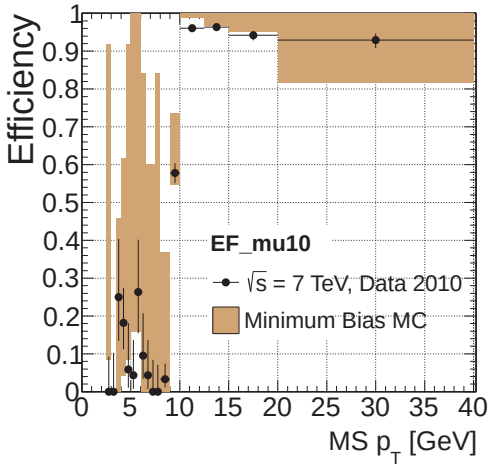

(f) *The* `EF_mu10` *trigger.*

Figure 3.6: *The L2 and EF turn-on curves for* `mu4` *(a,b),* `mu6`*(c,d) and* `mu10`*(e,f) triggers. For the L2, the efficiency is estimated relative to the L2 Muon Spectrometer trigger and with respect to the offline combined track* p_{T}*. For the EF, the efficiency is estimated relative to the L2 combined trigger and with respect to the offline combined track* p_{T}*.*

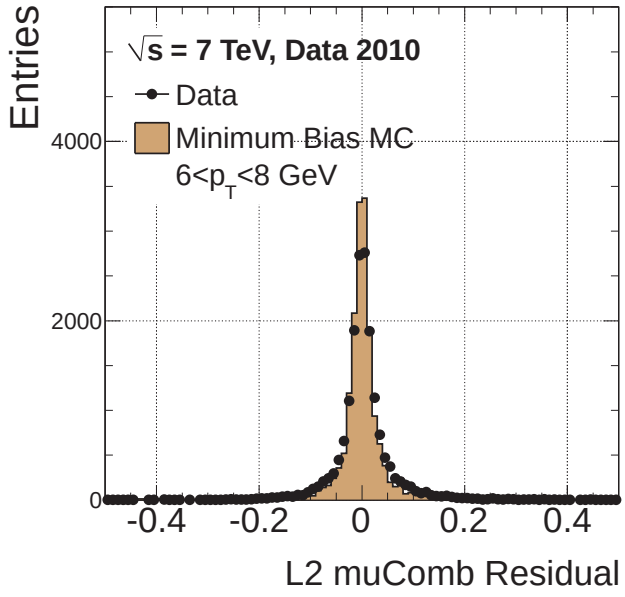

Figure 3.7: *Residual distribution of the transverse momentum calculated with equation 3.2.4 using as $p_{\mathrm{T}}^{offline}$ the measurement for the combined offline track and as $p_{\mathrm{T}}^{trigger}$ the measurement from the* `muComb` *algorithm.*

This approach, which is the easiest, is only possible when the events are unbiased from any kinematic cuts. In practice, as the instantaneous luminosity of the accelerator increases, the events that are written out are based on stricter trigger requirements and may be significantly biased. In this case, the easiest approach is to use Monte Carlo samples and apply the estimate directly to the analysis of interest. However, it is preferable to use data-driven techniques to avoid systematical uncertainties related with the simulation. Several data-driven methods exist:

- **Orthogonal triggers:** With this method the events are first selected based on a chain of algorithms A and are subsequently used to determine the efficiency of a second chain of algorithms B. For the measurement to be unbiased, A and B must be completely uncorrelated so that their efficiencies follow the relation $\epsilon_{A+B} = \epsilon_A \cdot \epsilon_B$. The following then holds:

$$N_A = \epsilon_A \cdot N_{all} \qquad \text{and}$$
$$N_{A+B} = \epsilon_B \cdot \epsilon_A \cdot N_{all} \ ,$$

  with N_{all} being the total number of events under consideration, N_A being the number of events left after using trigger A, and N_{A+B} when applying both trigger A and B. The efficiency of trigger B is then simply given by:

$$\epsilon_B = \frac{N_{A+B}}{N_A}.$$

  An important advantage of the orthogonal triggers method is that it can be applied on complex final states that have many different physics objects as these events may easily end-up in various physics streams. An example is the $t\bar{t}$ semi-leptonic events where one can trigger on the multiplicity and the high-p_{T} of the jets and subsequently measure the single-lepton trigger efficiency.

- **Tag-and-probe:** This method relies on collecting a sample of double-object final states where these objects are of the same kind. For example, such physics processes are the

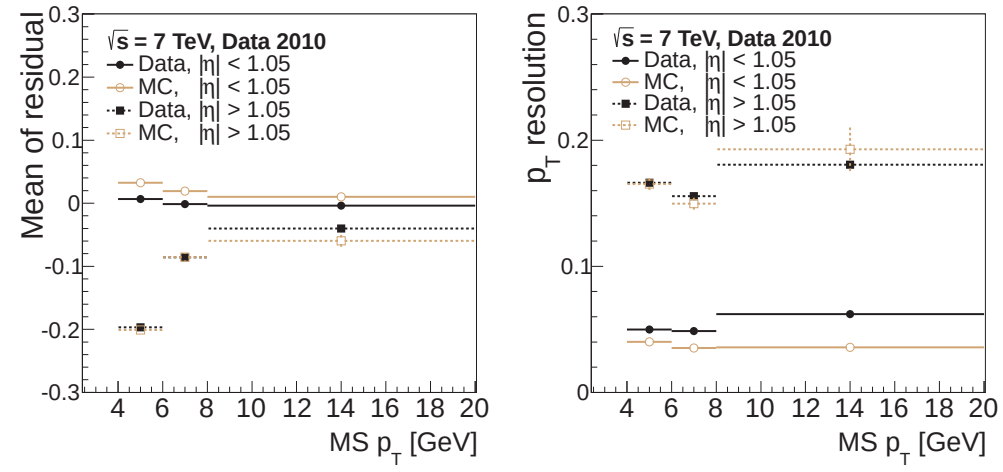

(a) *L2* `muFast` *distributions*

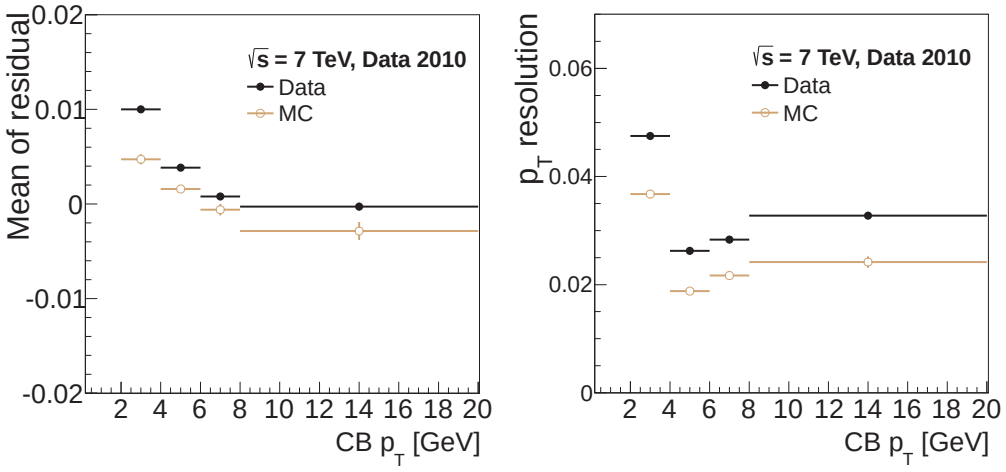

(b) *L2* `muComb` *distributions*

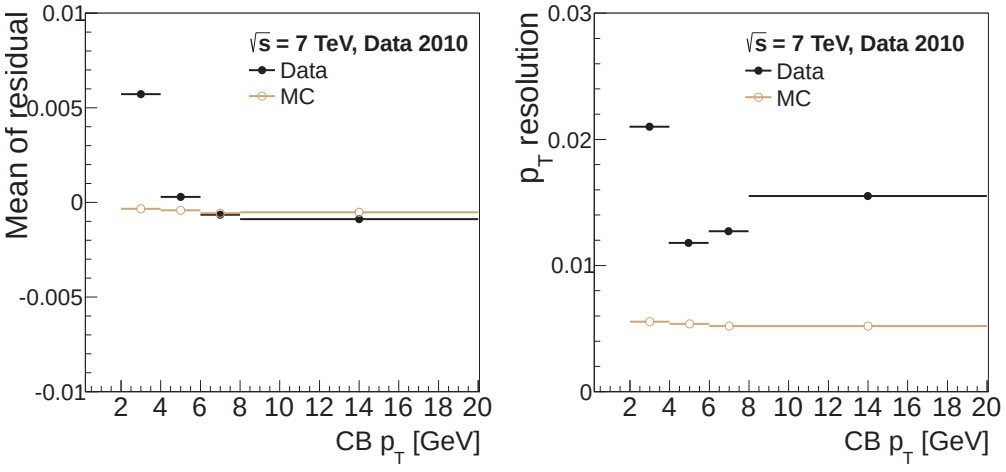

(c) *EF* `TrigMuonEF` *distributions*

Figure 3.8: *The residual mean (left) and the resolution (right) for different trigger algorithms as estimated by fitting the result on equation 3.2.4 at different p_{T} ranges. For the* `TrigMuonEF` *the combined track measurement is used.*

Z decay and the J/ψ decay which both result into two charged leptons which are also kinematically correlated. In this case, the signature is identified based on the two leptons and by estimating the invariant mass of the mother particle. However, only one of the leptons is used to trigger the events while the other is used to determine the trigger efficiency.

- **Bootstrap:** The bootstrap method requires the knowledge of a trigger's turn-on curve behavior, trigger A (ϵ_A), and provides an estimate on the efficiency of a second trigger, trigger B (ϵ_B), which has a higher threshold than A. Both triggers should be of the same type and events triggered by B must be triggered by A as well. The efficiency of B can be estimated with the following:

$$\epsilon_B = \epsilon_A \cdot \left[\frac{\epsilon_B}{\epsilon_A}\right],$$

where the fraction $[\epsilon_B/\epsilon_A]$ is equivalent to the ratio of events N_B/N_A and therefore is estimated by counting the corresponding event yield. Namely, those that passed trigger B, and therefore A as well, are divided by the total of those that passed trigger A. The main advantage of the bootstrap method is that it can provide an estimate of the efficiency for triggers with significantly high thresholds that would typically be used for rare physics signatures. Its reliance on the knowledge of the behavior of trigger A is important but this behavior can be determined with the use of a tag-and-probe technique.

From the above methods, the tag-and-probe is the one that is exploited the most as it uses physics signatures that are abundantly produced by the LHC. In the rest of this section this method is discussed in more detail and is applied on a dataset collected during 2010.

3.3.1 Description of the tag-and-probe method

As mentioned previously, the tag-and-probe (T&P) method is based on selecting an event sample that contains two correlated objects of the same type. Here, we apply this method to Z events that decay to two muons, namely:

$$Z \to \mu^+\mu^-.$$

These events provide energetic muons that are well isolated and kinematically very similar to muons originating from $t\bar{t}$ leptonic decays. The latter are of interest in this thesis as they are considered for the cross-section measurement presented in the next chapters.

The method can be summarized as follows. Events are selected at the trigger level by requiring the trigger, which is of interest for the measurement, to have fired; the trigger should have a multiplicity requirement of at least one and a p_{T} threshold that is consistent with what is expected from a Z decay. At the offline level, two muons of opposite charge are required to be present, both satisfying the same set of kinematic cuts. Combined, they should have an invariant mass within a mass-window around the true Z mass. If di-muon invariant mass is compatible with the Z mass, one of the muons is required to have fired the trigger and is then flagged as the 'tag'. The fact that events are selected with the trigger that is examined ensures that at least one of the muons fulfills this requirement. Subsequently, the second muon is considered as the 'probe' and the trigger efficiency can be examined by checking whether it has fired the trigger as well.

Mathematically we can formulate the method by forming two event samples. The first sample is after the tag selection where at least one muon is required to have passed the trigger:

$$N_{1\mu} = \epsilon_{1\mu}^{trig} \cdot \epsilon_{sel} \cdot N_{all}, \tag{3.3.1}$$

where ϵ_{sel} is the selection efficiency of the events based on the offline cuts and includes the reconstruction efficiency of the Z boson, $\epsilon_{1\mu}^{trig}$ is the efficiency with which the trigger selects these events by requiring at least one muon to have fired, and N_{all} is the total number of events under consideration.The second sample is after requiring that the probe muon has also passed the trigger, thus:

$$N_{2\mu} = \epsilon_{2\mu}^{trig} \cdot \epsilon_{sel} \cdot N_{all}, \tag{3.3.2}$$

where $\epsilon_{2\mu}^{trig}$ is again the efficiency with which these events are triggered based on both muons having passed the trigger requirements.

The efficiencies $\epsilon_{1\mu}^{trig}$ and $\epsilon_{2\mu}^{trig}$ are not equivalent but are related to the absolute trigger efficiency (ϵ_{trig}), which is of interest as explained in the next paragraph. Seen as a probability per event, in which two muons exist (μ_1 and μ_2), the parameters $\epsilon_{1\mu}^{trig}$, $\epsilon_{2\mu}^{trig}$ can be written in the following form:

$$\begin{aligned} P_{1\mu} &= P(\mu_1, \bar{\mu_2}) + P(\bar{\mu_1}, \mu_2) + P(\mu_1, \mu_2), \\ P_{2\mu} &= P(\mu_1, \mu_2). \end{aligned} \tag{3.3.3}$$

where $P(\mu_1, \bar{\mu_2})$ is the probability with which μ_1 is accepted by the trigger when μ_2 is rejected, $P(\bar{\mu_1}, \mu_2)$ where μ_1 is rejected while μ_2 is accepted, and $P(\mu_1, \mu_2)$ is the probability where both are accepted. These can be written as follows:

$$\begin{aligned} P(\mu_1, \bar{\mu_2}) &= P(\mu_1) \cdot [1 - P(\mu_2)], \\ P(\bar{\mu_1}, \mu_2) &= P(\mu_2) \cdot [1 - P(\mu_1)], \text{ and} \\ P(\mu_1, \mu_2) &= P(\mu_1) \cdot P(\mu_2). \end{aligned} \tag{3.3.4}$$

where $P(\mu_1)$ and $P(\mu_2)$ are the probabilities of μ_1 or μ_2 respectively to pass the trigger requirement and which are equivalent. Therefore, following from the equations 3.3.3 and 3.3.4 we can write:

$$\begin{aligned} P_{1\mu} &= \epsilon_{1\mu}^{trig} = 2 \cdot \epsilon_{trig} - \epsilon_{trig}^2, \\ P_{2\mu} &= \epsilon_{2\mu}^{trig} = \epsilon_{trig}^2. \end{aligned} \tag{3.3.5}$$

By substituting the result of the equations 3.3.5 to equations 3.3.1 and 3.3.2 we have the following relation for the absolute trigger efficiency:

$$\epsilon_{trig} = \frac{2 \cdot N_{2\mu}}{N_{1\mu} + N_{2\mu}}. \tag{3.3.6}$$

The result of equation 3.3.6 is equivalent with what we would obtain by simply counting the rate of probes that successfully pass the trigger criteria over the total number of probes, namely:

$$\epsilon_{trig} = \frac{N_{\text{triggered probes}}}{N_{\text{all probes}}}. \tag{3.3.7}$$

In this case, it should be taken into account that when a probe is successful in firing the trigger, the event has two possible permutation of tag and probe muons. Both of these cases must be considered in order to avoid the bias due to the selection of the tag.

3.3.2 Data sample and event selection for the T&P

The data sample used for performing this measurement is not the same as the one in section 3.2.1. A number of interventions were made after the first data were collected, which improved the performance of the trigger system. In addition, the higher luminosity in later periods provided a larger number of events in subsequent periods. The data sample that is used contains events that were recorded with the detector fully operational from period E4 up to and including the end of period F, and is estimated to a total of 2.04 pb^{-1}; see table 3.6.

Period	$\int \mathcal{L}dt$ (nb^{-1})	Date (in 2010)
E (4-7)	510	6^{th} August - 18^{th} August
F (1-2)	1530	19^{th} August - 30^{th} August
All Periods	2040	

Table 3.6: *Total integrated luminosity registered by ATLAS for the data periods included in the T&P analysis in this thesis.*

Event selection

The selection of events for the T&P analysis starts by requiring the events to have passed the `EF_mu10_MSonly` trigger chain. This is also the trigger for which the efficiency will be measured as it was chosen as the primary trigger for the $t\bar{t}$ analyses that involve a muon in their final states. In the following chapters of this thesis (where the $t\bar{t}$ cross-section measurement is discussed), this trigger was used for the periods from E4 until F. A positive decision on the `EF_mu10_MSonly` implies that the corresponding L2 trigger (`L2_mu10_MSonly`) and L1 item (`L1_MU0`) have also given a positive response, the final efficiency is therefore cumulative for all the trigger levels.

At the offline level, for identifying the Z decays, each event must successfully pass the following requirements:

- A primary vertex reconstructed with at least three tracks associated with it in order to reject the non-collision background.
- The number of accepted reconstructed muons must be exactly two ($N_\mu = 2$) and they must be of opposite charge.

Not all muons are considered in the above selection. Each muon must fulfill the following requirements:

- Muons must be reconstructed by the `MuID` reconstruction and be classified as *"tight"* with a combined track. The "tight" classifications requires the muon to fulfill the logical `OR` of having a `MuID` combined track, having a `MuID` standalone track for when $|\eta| > 2.5$ and having a `MuGirl` extended track. The explicit requirement in our selection for a combined track refines this definition, aiming to increase the purity of the final sample. The muon reconstruction and its track quality definitions are also discussed in the following chapter, in section 4.1.2, and in more detail under the context of the $t\bar{t}$ cross-section analysis.
- The quality of the Inner Detector track of the combined muon must also be ensured. This requires a set of cuts to be applied, namely:
  i. A hit on the B-layer of the Inner Detector is required, unless the muon track has passed an un-instrumented or dead-area of this sub-detector.

ii. The number of hits in the Pixel layers plus the number of crossed dead pixel sensors must be $N_{Pixel} + N_{dead,Pixel} > 1$.

iii. The number of hits in the SCT layers plus the number of crossed dead SCT sensors must be $N_{SCT} + N_{dead,SCT} > 5$.

iv. The number of Pixel and SCT layers traversed by the track but with no hits (holes) must be, $N_{holes,Pixel} + N_{holes,SCT} < 2$.

v. Lastly, for the region that is covered by the TRT, if we define:

$$N_{TRT} = N_{TRT}^{hits} + N_{TRT}^{outliers},$$

then we require that:

$$\text{for } |\eta| < 1.9 : N_{TRT} > 5 \text{ and } \frac{N_{TRT}^{outliers}}{N_{TRT}} < 0.9,$$

$$\text{for } |\eta| \geq 1.9 : \frac{N_{TRT}^{outliers}}{N_{TRT}} < 0.9 \text{ only if } N_{TRT} > 5.$$

- The transverse momentum of the muon must be $p_{\mathrm{T}} > 20$ GeV. This requirement puts the muon far from the turn-on slope and within the expected plateau of the trigger's turn-on curve.
- It should lie within $|\eta| < 2.5$, which is the acceptance of the Inner Detector.
- Lastly, the muon should be well isolated and this is ensured by the following requirements:
  i. The calorimetric and tracking isolation parameters should both be less than 4 GeV. The definition of these parameters stipulates that a cone with an opening angle of 0.3 in $\eta - \phi$ space around the muon track is defined. For the calorimetric isolation, the energy deposited on the calorimeter within the cone and excluding the muon itself should be less than 4 GeV. Similarly, the tracking isolation, estimates the scalar sum of the p_{T} of all tracks within the cone and, excluding the muon, requires that is less than 4 GeV. Both isolation variables are also discussed in the next chapter in section 4.1.2 as they are also used for the cross-section analysis.
  ii. The distance of the muon with respect to the closest reconstructed jet with a $p_{\mathrm{T}} > 20$ GeV must be $\Delta R(\mu, \text{closest jet}) > 0.4$. Reconstructed jets are created with the `anti-`$k_{\perp}$ [126] using a jet size of 0.4 and are calibrated with the `EMJES` scheme [127]. The jet reconstruction and calibration is discussed in greater detail in the next chapter in section 4.1.3.

The definitions for both muons and jets in this selection are motivated by the selection that is applied for the $t\bar{t}$ cross-section measurement that is described in the following chapters.

After identifying the muon sample, the tag and the probe muons are specified

- **Tag:** For an offline reconstructed muon to be considered a tag, it must be matched to a trigger object that satisfies the `EF_mu10_MSonly` threshold. The matching requirement is $\Delta R < 0.3$.
- **Probe:** For the second muon in the event to be considered as a probe, the reconstructed di-muon invariant mass must give a result compatible with the Z boson mass pole. In particular, it must hold that $|M_{\mu^+\mu^-} - M_Z| \leq 12.5$ GeV, where the M_Z is 91.1876±0.0021 [53]. The choice of the 12.5 GeV threshold is made such that the acceptance window is roughly ten times the decay width of the boson ($\Gamma_Z = 2.4952$ GeV [53]), thus reducing significantly the probability of a true Z boson to be excluded because its mass is found deviated from the lineshape's peak.

The above selection selects an almost pure sample of Z bosons as is also evident by the invariant mass distribution of the muon pair which is shown in figure 3.9. The agreement with Monte Carlo is good, indicating that any background contributions is negligible. A total of 1114 probes are collected from which 541 are found in the barrel region ($|\eta| < 1.05$) and 573 in the end-caps ($1.05 \leq |\eta| < 2.4$). The kinematic distributions of the probes are shown in figure 3.10 and again a good agreement with the Monte Carlo is observed.

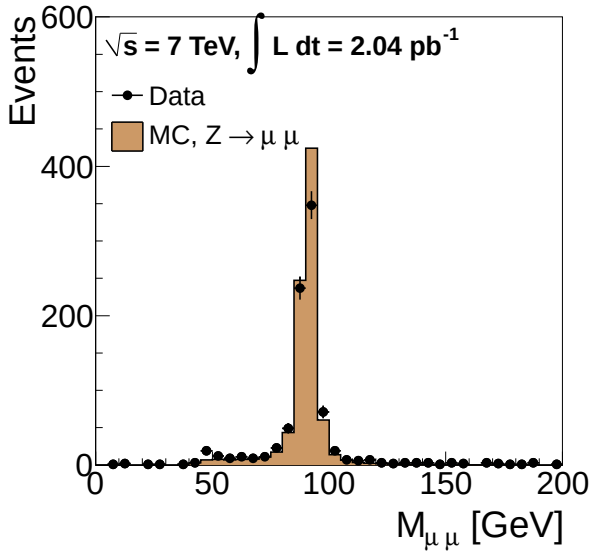

Figure 3.9: *Invariant mass distribution of the muon pair after the tag and probe event selection requirements. The Monte Carlo $Z \to \mu^+\mu^-$ is also drawn.*

3.3.3 Results

The efficiency of the `EF_mu10_MSonly` trigger as obtained by counting the probes that have fired this trigger is shown in table 3.7. We expect the difference between data and Monte Carlo to be caused by effects explained in section 3.2.2 such as the L2 LUT optimization.

In figure 3.11 the efficiency is shown with respect to p_{T}, η and ϕ. The data and Z boson Monte Carlo efficiency is obtained from the probe muons after applying the T&P method. It is clear that the amount of statistics does not leave room for a refined binning, however it still possible to observe the reduced plateau efficiency of the p_{T} distribution in the barrel, compared to the one measured in the end-caps, which is attributed to the complex geometry of the Muon Spectrometer in that pseudo-rapidity region; this is in agreement with the performance measurements presented earlier. The complex geometry also affects the η and ϕ distributions, with the most striking example in the negative ϕ region where the 'feet' of the detector are located. Overall, the data and Monte Carlo agreement is good and in certain bins where large fluctuation are observed, as in example in the region of $-0.8 < \eta < -0.6$. These are attributed to the limited statistics.

Z boson decays vs. $t\bar{t}$ decays

An important question that arises after measuring the efficiency using Z decays, is whether this number is applicable to other physics processes as well. The events that are of interest in this thesis are the $t\bar{t}$ leptonic decays and the muons that originate from the W boson decay are expected also to be well isolated and in general kinematically equivalent to muons coming from Z bosons. However, $t\bar{t}$ events exhibit differences in their signature with respect to the Z boson events and most notably in their jet activity which is much higher. To make sure that the T&P analysis result is valid for $t\bar{t}$ events, the efficiency of muons originating from decaying

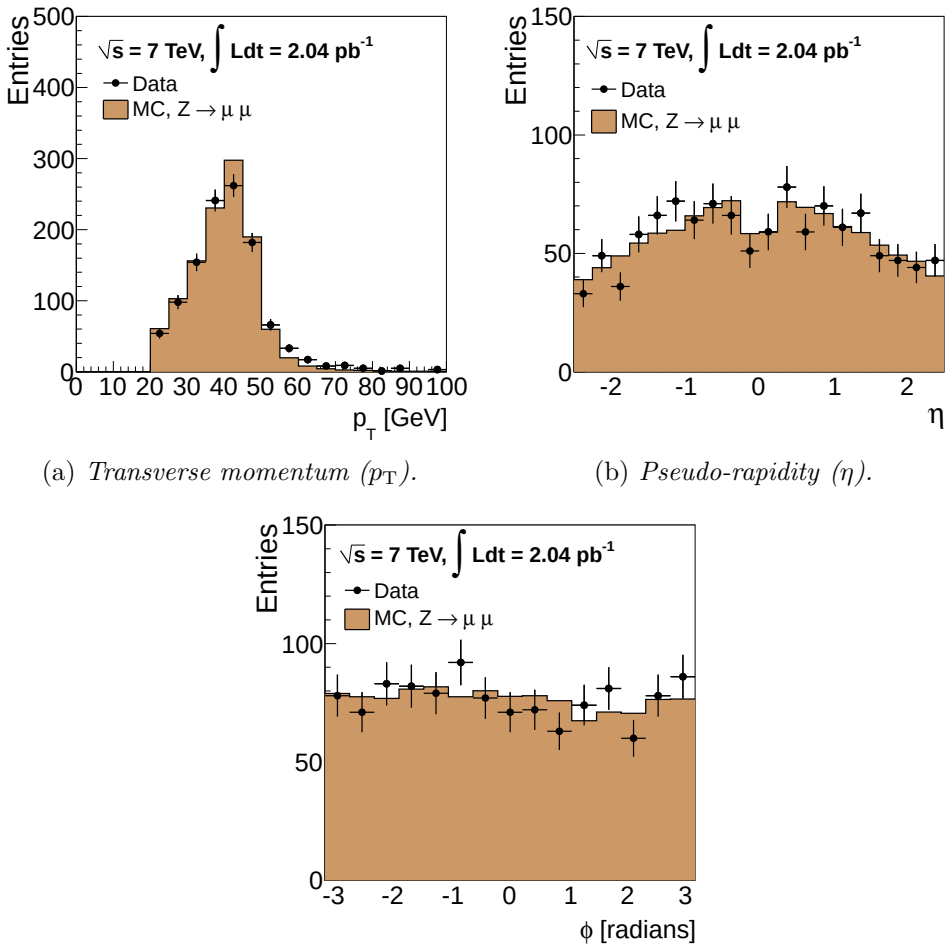

(a) *Transverse momentum (p_{T}).*

(b) *Pseudo-rapidity (η).*

(c) *Azimuthal angle (ϕ).*

Figure 3.10: *The p_{T}, η and ϕ of the probe muons selected with the T&P selection requirements. A total of 1138 probes are collected.*

Detector Region	**Efficiency**	
	Monte Carlo	Data
Barrel ($\lvert\eta\rvert < 1.05$)	$75.02^{+0.12}_{-0.13}\%$	$70.05^{+1.94}_{-1.99}\%$
End-caps ($1.05 < \lvert\eta\rvert < 2.4$)	$93.61^{+0.09}_{-0.09}\%$	$90.92^{+1.15}_{-1.24}\%$
Full coverage ($\lvert\eta\rvert < 2.4$)	$84.33^{+0.08}_{-0.08}\%$	$80.79^{+1.16}_{-1.20}\%$

Table 3.7: *Overall trigger efficiency for* `EF_mu10_MSonly` *as obtained with the T&P method. The quoted uncertainties are statistical only.*

top quarks is also plotted in figure 3.11. As with the Z muons, these are also required to pass object selection requirements mentioned earlier. The agreement between the Z boson Monte Carlo and the $t\bar{t}$ is very good, suggesting that there is no need for further correction.

Application of the extracted efficiency to analyses

Finally, after determining the trigger efficiency with the described method, it must be applied on the analysis of interest. This usually happens not by directly applying it on the final

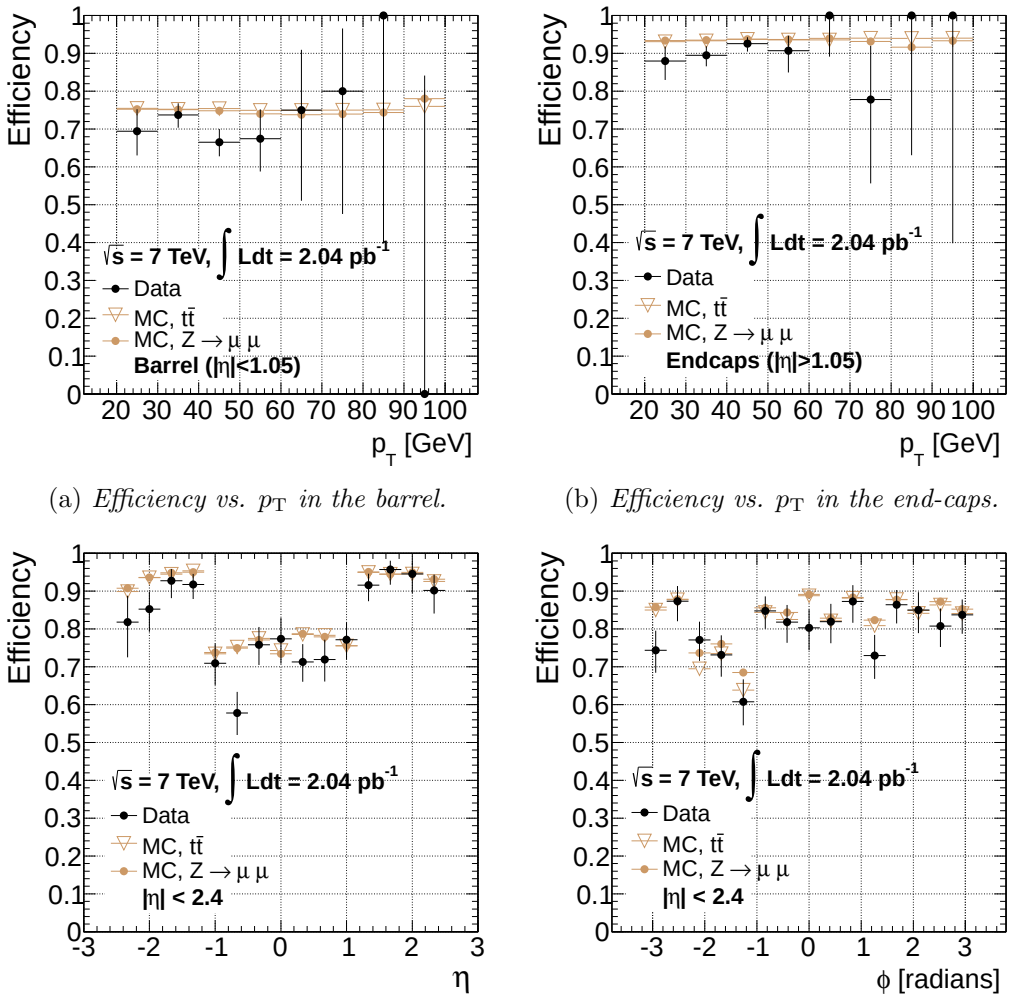

(a) *Efficiency vs.* p_{T} *in the barrel.*

(b) *Efficiency vs.* p_{T} *in the end-caps.*

(c) *Efficiency vs.* η.

(d) *Efficiency vs.* ϕ.

Figure 3.11: *Efficiency with respect to the probe muon's* p_{T} *in the barrel (a) and end-cap (b) regions as well as with respect to its* η*(c) and* ϕ *(d) co-ordinates. The estimate from Monte Carlo* Z *boson decays is plotted and also the efficiency as obtained by muons coming from* $t\bar{t}$ *decays.*

measurement but instead by expressing it in the form of a scale factor which is defined as follows:

$$SF = \frac{\epsilon_{data}}{\epsilon_{MC}}, \tag{3.3.8}$$

where ϵ_{data} is the efficiency as obtained from the data-driven method and ϵ_{MC} is the efficiency as obtained from the Monte Carlo. The main advantage of this is that one could simply take the uncertainty on the scale factor which is less sensitive to systematic variation than the efficiency itself. As will be discussed in chapter 6, this approach is preferred for the analysis performed in this thesis.

For the results shown above, the scale factor is expressed separately for the barrel and the end-cap regions; see table 3.8. The total systematic uncertainty quoted in the final result is taken after adding in quadrature the variation of the scale factor from each of the following sources:

Detector Region	Scale Factor
Barrel ($\|\eta\| < 1.05$)	$0.934^{+0.026}_{-0.027}(stat.)^{+0.012}_{-0.008}(syst.)$
End-caps ($1.05 < \|\eta\| < 2.4$)	$0.971^{+0.012}_{-0.013}(stat.)^{+0.010}_{-0.016}(syst.)$

Table 3.8: *Resulting trigger scale factors from T&P for the* `EF_mu10_MSonly` *trigger during the data periods E4-F2.*

- **Mass-window:** The choice of the 12.5 GeV mass-window is based on the decay width of the Z boson. We test the sensitivity of our result by changing the threshold by 2.5 GeV to both higher and lower values.
- **Offline-to-trigger matching:** Determining that an offline muon has fired the trigger, happens by matching it to a trigger object that passes these requirements. The choice of the matching threshold is tested by altering it by 0.2 both upwards and downwards.
- **Tag isolation criteria:** Lastly, the choice of the isolation criteria and their effects on the scale factor is examined in a rather conservative way by completely removing these requirements, namely the calorimetric and tracking isolation as well as the overlap removal with the close-by jet.

3.4 Summary

In this chapter the triggering of muon particles was thoroughly discussed. With the first data recorded by the detector it was possible to assess the performance of the muon trigger and identify problems that would help in the commissioning of the detector. All of the problems that were encountered have been addressed for the subsequent data taking periods. In addition, as the trigger system is the first event selection layer in an analysis, it is imperative that its efficiency is known during data-taking. With the increase of the instantaneous luminosity of the LHC, the selected events become biased by the selection of the trigger and therefore direct estimation of its efficiency is not possible. The tag-and-probe method provides a data-driven method that allows the measurement of the muon trigger efficiency also for muons that originate from $t\bar{t}$ decays. The result from this method was obtained and presented for the `EF_mu10_MSonly` trigger that was used during the data periods E4-F2 for the top-related analysis.